Acta Materialia 208 (2021) 116679

Contents lists available at ScienceDirect

Acta Materialia

journal homepage: www.elsevier.com/locate/actamat

Thermal stability of immiscible Cu-Ag/Fe triphase multilayers with triple junctions

Tongjun Niu[a], Yifan Zhang[a], Jaehun Cho[a], Jin Li[b], Haiyan Wang[a,c], Xinghang Zhang[a,*]

[a] School of Materials Engineering, Purdue University, West Lafayette, IN, 47907, USA
[b] Institute of Special Environments Physical Sciences, Harbin Institute of Technology, Shenzhen 518055, China
[c] School of Electrical and Computer Engineering, West Lafayette, IN, 47907, USA

ARTICLE INFO

Article history:
Received 31 July 2020
Revised 17 January 2021
Accepted 18 January 2021
Available online 21 January 2021

Keywords:
Triphase
Triple junction
Thermal stability
Grooving kinetics

ABSTRACT

Nanostructured metallic multilayers have attracted significant attention due to their high mechanical strength. However, they often have limited thermal stability at elevated temperatures. Multilayers with immiscible constituents also suffer from high temperature microstructure instability due to thermal grooving and subsequent layer pinch-off. Here we report the enhanced thermal stability of immiscible triphase Cu-Ag/Fe multilayer with triple junctions comparing to Cu/Fe multilayers. The immiscible Cu/Fe multilayers experienced drastic thermal grooving and rapid grain growth at 500°C, followed by the complete breakdown of layer structure and spheroidization at 600°C. In comparison, the layer structures of Cu-Ag/Fe triphase multilayers remain stable up to 600°C with insignificant grain coarsening. The grooving kinetics as well as the underlying mechanisms that lead to the excellent thermal stability of the triphase multilayers are discussed. This study provides a fresh perspective on designing thermally stable nanostructured multilayers for high temperature applications.

1. Introduction

Nanostructured metals have attracted intense research interest due to their high strength [1–10], good wear resistance [11–14] and superior radiation tolerance [15–19]. However, their high interface-to-volume ratio makes them vulnerable to high temperature microstructure instabilities driven by the minimization of excess free energy of grain boundaries (GBs) [20–23]. The poor thermal stability is manifested by the property degradation at elevated temperature, for instance, the loss of high strength of nanocrystalline metals due to rapid grain coarsening [24]. A variety of strategies have been applied to stabilize nanostructured metals from both kinetics and thermodynamics perspective [25–28]. For example, second phase particles can exert the Zener pinning effect on the migration of GBs and thus slow down grain coarsening [29–31]. The addition of solutes is also proven to be beneficial as the solutes can either drag the interface movement or lower the GB energy via GB segregation [32–36].

Nanostructured metallic multilayers often exhibit unique high temperature behavior arising from their architectures [37–40]. For multilayers with miscible components, the microstructure evolution at elevated temperature is dominated by the interdiffusion across layer interface, leading to the intermixing and formation of intermetallic phases [41–44]. In contrast, for multilayers with immiscible constituents, the limited miscibility restrains the interdiffusion across the layer interface, and the microstructure evolution is governed by the mass transport within individual layers and along the layer interfaces [45–48]. Previous studies showed that the lamellar structure with single crystal layers could suffer from high temperature microstructure instability in the form of edge spheroidization [46], boundary splitting [47,49] and termination migration [50,51]. For multilayers with polycrystalline structure, one major instability mechanism is the development of thermal grooving at the intersection between grain boundaries and interphase boundaries [45,48,52,53].

The development of grooving in polycrystalline multilayers is governed by the local composition, grain structure and layer thickness [39,54,55]. The equilibrium grooving angle ($2\theta_{eq.}$) at the triple junction where grain boundaries intersect with phase boundaries is determined by the ratio between GB energy (γ_{gb}) to phase boundary energy (γ_{pb}) via [54]:

$$\cos\theta_{eq}=\frac{\gamma_{gb}}{2\gamma_{pb}} \quad (1)$$

when θ_{eq} value is small, the grooves tend to grow and penetrate through the layers, leading to the layer pinch-off. In contrast, a larger θ_{eq} normally comes along with little grooving and a more

* Corresponding author.
E-mail address: xzhang98@purdue.edu (X. Zhang).

https://doi.org/10.1016/j.actamat.2021.116679
1359-6454/

stable lamellar structure. Furthermore, both experimental observations and simulation studies reveal the important role of grain aspect ratio, h/d, in controlling the thermal stability of multilayers [48,56], where h is the layer thickness, d is the in-plane grain size. The breakdown of the layer structure is favored when h/d is small since the groove depth at the same θ_{eq} will increase with the increasing diffusion distance between the two consecutive grooves [55]. Recent studies on thermal stability of Hf/Ti [57], Cu/Ru [58], and Cu/Co [59] multilayers suggest that columnar structures with large grain aspect radio typically exhibit enhanced thermal stability comparing to the pancake-like structures with smaller aspect ratio. Therefore, a general criterion to stabilize the layer structure is to increase the h/d ratio [45].

Despite the detrimental effect of thermal grooving on layer structure stability, previous studies by Mullins and Frost *et al.* show that the groove development at triple junctions can drag the migration of GB and prohibit significant in-plane grain growth [60,61]. In addition, Misra et al. discovered that the grooving led to the zig-zag alignment of triple junctions in Cu/Nb multilayers upon high temperature annealing. The triple junctions were offset by shear and anchored with each other, forming the zig-zag pattern [55,62]. Such zig-zag structure exhibited superb thermal stability and no layer pinch-off occurred at 700°C up to 60 hours [62].

In this study, we investigate the thermal stability of immiscible Cu-Ag/Fe multilayer with triphase triple junctions. The microstructure evolutions of triphase Cu-Ag/Fe multilayer were systematically studied via transmission electron microscopy (TEM) and energy dispersive X-ray spectroscopy (EDS). Factors that contribute to the stabilization of layer structure are discussed. The grooving kinetics was evaluated using a modified Mullins' model. The enhanced resistance to thermal grooving and layer pinch-off by triphase Cu-Ag/Fe multilayers may provide new insights on the design of thermally stable nanostructured multilayers.

2. Experimental

Cu-Ag/Fe 100 nm and Cu/Fe 100 nm multilayers with equal individual layer thickness were deposited on oxidized Si substrates using DC magnetron sputtering at room temperature. The stoichiometric $Cu_{70}Ag_{30}$ (at.%) layers were co-sputtered using elemental Cu (99.99%) and Ag (99.998%) targets. The chamber was evacuated to a base pressure of 8×10^{-8} torr prior to deposition. Annealing experiments were performed in vacuum furnace with a base pressure of 2×10^{-6} torr over 200-600°C for 1 hour, followed by subsequent furnace cooling. X-ray diffraction (XRD) experiments were performed on a Panalytical Empyrean system (Cu Kα radiation) at room temperature. Cross-sectional transmission electron microscopy (XTEM) samples were mechanically grinded and polished, followed by dimpling and low energy Ar ion milling by a Gatan PIPS II system. TEM experiments were performed on a Thermo Fischer Scientific/FEI Talos 200X microscope with Super-X EDS detectors operated at 200 kV. The average grain size is measured using the XTEM specimens by the line interception method [63]. In particular, we coupled the bright field TEM and scanning transmission electron microscopy (STEM) images with EDS mapping to measure the grain size of Cu and Ag.

3. Results

Fig. 1a shows the XTEM micrograph and corresponding selected area diffraction (SAD) pattern of the as-deposited Cu/Fe 100 nm multilayer. The inset SAD pattern with discontinuous diffraction rings reveals the polycrystalline nature of Cu/Fe multilayer. EDS map in Fig. 1b displays the chemically sharp Cu/Fe layer interface. As shown in Fig. 1c, the Fe layers are composed of nanoscale columnar grains. The statistical analyses in Fig. 1d show that the average column size in Fe layers is 18 nm. In contrast, the average column size in Cu layers is 45 nm, much greater than that in Fe layers.

Fig. 2a shows the cross-sectional microstructure of the as-deposited Cu-Ag/Fe 100 nm multilayer. Due to the positive heat of mixing and large miscibility gap, the co-sputtering of Cu and Ag at room temperature produced a supersaturated nanocrystalline structure with fine grain size (less than 10 nm). No amorphous ring was observed in the inserted SAD pattern (Fig. 2a). Fig. 2b shows the periodical chemical distribution of Cu-Ag/Fe multilayer. Fig. 2c reveals the columnar structure in Fe layers. The inset high resolution TEM (HRTEM) micrograph taken at layer interface in Fig. 2c further confirms the crystalline structure of the $Cu_{70}Ag_{30}$ layers. The average column size of Fe layers is 27 nm as shown in the histogram in Fig. 2d. The dark field (DF) TEM image in Fig. 2e reveals the substructures in $Cu_{70}Ag_{30}$ layers. The diffraction ring used for acquiring the DF image is marked by the red dashed circle.

Fig. 3a compiles the XRD profiles of both as-deposited and annealed (up to 600°C) Cu/Fe 100 nm multilayers. The Fe layers exhibit a strong bcc (110) texture while Cu layers has pronounced (111) texture. XRD patterns of Cu-Ag/Fe 100 nm multilayers annealed at different temperatures are shown in Fig. 3b. The magnified XRD profile of as-deposited Cu-Ag/Fe multilayer in Fig. 3c shows two broad low-intensity peaks over 38°-40° and 41°-43° due to the mixture of supersaturated Cu and Ag nanograins. It is intriguing to note that the peak width for both Cu/Fe and Cu-Ag/Fe multilayers decreased with the increasing annealing temperature, suggesting the occurrence of grain coarsening.

Fig. 4 shows the microstructure evolution of Cu/Fe multilayer annealed up to 600°C. As shown in Fig. 4a and c, the Cu/Fe layer interfaces remained flat and intact while both the Cu and Fe columnar grains coarsen after annealing at 200 and 400°C. Evident grooving and substantial in-plane grain growth took place after 500°C annealing as shown in Fig. 4e. Annealing at 600°C led to the breakdown of the layer structure as the grooves develop rapidly and eventually penetrate through the layer interfaces (Fig. 4g). Thereafter, the discontinuous layers suffered from rapid spheroidization and quickly evolved into giant grains as indicated by the yellow arrows in the EDS map in Fig. 4h.

The microstructure evolution of Cu-Ag/Fe multilayers at different annealing temperature was examined by TEM coupled with EDS mapping analyses. Annealing at 200°C resulted in the formation of discernable grain boundaries and phase boundaries between Cu and Ag grains (Fig. 5a). EDS map in Fig. 5b indicated the demixing of Cu and Ag. As shown in Fig. 5c, the layer interfaces remained straight after 400°C annealing. The complete phase separation of Cu and Ag was observed at 500°C (Fig. 5e). In addition, insignificant roughening of the layer interface was observed. After 600°C annealing, comparing to the complete breakdown of layer structures in Cu/Fe multilayer, the layer structure of the Cu-Ag/Fe multilayer remained intact without layer pinch-off (Fig. 5g).

Fig. 6 compares the grain size evolution of Cu and Fe upon annealing between Cu/Fe and Cu-Ag/Fe multilayers. No distinct grain size difference between the two multilayer systems was observed when annealing temperature is below 400°C. Notably, an abrupt grain growth in both Cu layers and Fe layers of Cu/Fe multilayer took place at 500°C, as indicated by the sudden increase of the slope of the blue curves (Fig. 6a-b). The average columnar grain sizes of Fe and Cu reach 175 and 163 nm, respectively. In contrast, the grain growth of both Cu grains and Fe grains in Cu-Ag/Fe multilayer was much less dramatic. The average grain sizes of Fe and Cu are 94 and 127 nm, respectively. The rapid grain coarsening in Cu/Fe multilayer proceeded continuously at 600°C, resulting in much more substantial grain size difference between the two systems. In the Cu/Fe multilayer after annealing at 600°C, the average

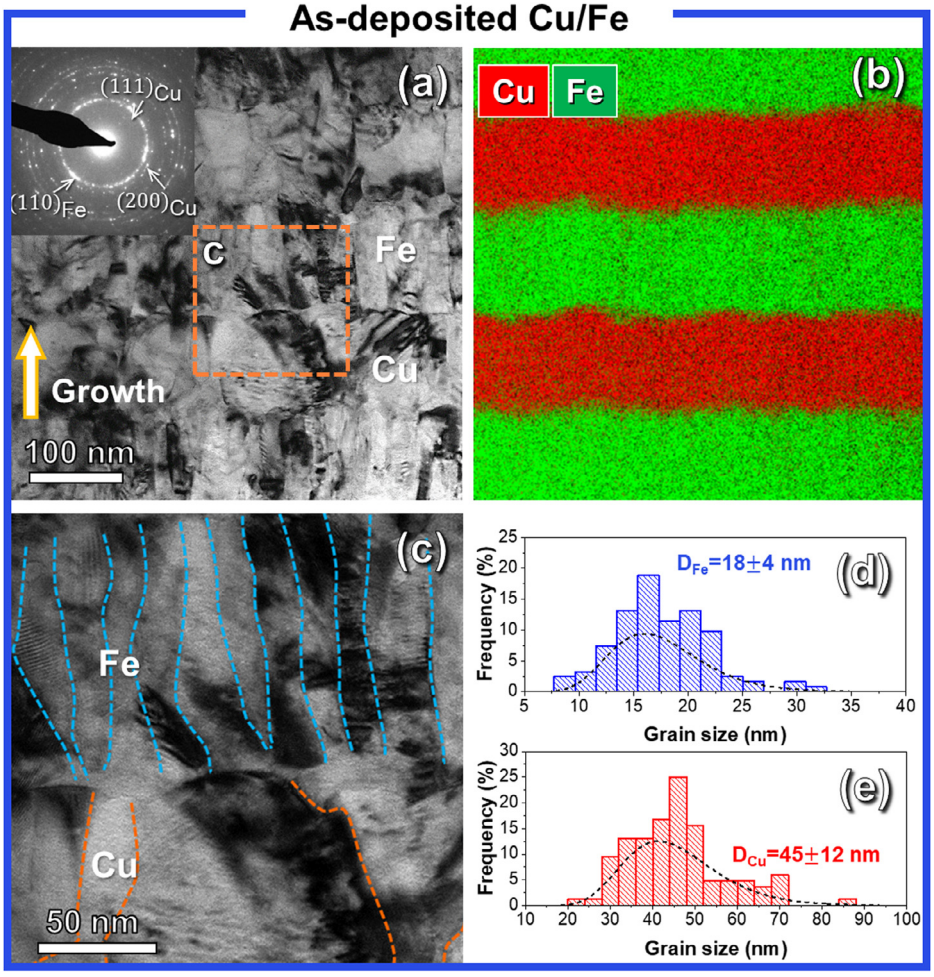

Fig. 1. Microstructures of as-deposited Cu/Fe 100 nm multilayer on SiO_2 substrate. (a) Cross-section TEM (XTEM) micrograph and the inserted selected area diffraction (SAD) pattern revealing the polycrystalline nature. (b) EDS map showing Cu in red and Fe in green. (c) A magnified view in box c reveals the formation of nanoscale columnar grains in Fe layers. (d-e) The statistical distributions show that the average grain sizes of Fe and Cu are 18 nm and 45 nm, respectively.

grain sizes of Fe and Cu increased to 280 and 260 nm, comparing to 126 nm for Fe and 169 nm for Cu in the annealed Cu-Ag/Fe multilayer.

4. Discussion

4.1. Microstructure evolution upon high temperature annealing

In both as-deposited Cu/Fe and Cu-Ag/Fe multilayers, the Fe layers display the fine columnar structure with in-plane grain sizes of 18 and 27 nm, respectively (Fig. 1). In contrast to the clearly discernable boundaries of Cu grains in Cu/Fe multilayers, the co-sputtering of Cu and Ag resulted in the extremely small subgrain size (less than 10 nm) in CuAg layers as evidenced by the DF TEM micrograph in Fig. 2e. Meanwhile, the SAD pattern indicates a {110}bcc and {111}fcc texture [55]. Despite the positive heat of mixing between Cu and Ag and a mutual equilibrium solid solubility below 1 at% at room temperature, previous studies on co-sputtered CuAg films reported that the limited atomic mobility during room temperature sputtering would favor the formation of supersaturated dual-phase CuAg alloy [64,65]. The alloying effect was found to greatly reduce the grain size of the metastable crystalline structure by a factor of 5-10 when compared with the pure elemental metals [65]. As shown in Fig. 3c, the subgrains and CuAg supersaturated solid solutions evoke two broad humps at 38°-40° and 41°-43° in the XRD pattern of the as-deposited Cu-Ag/Fe multilayer. Upon annealing, the solute atoms in the supersaturated phases (Ag atoms in Cu-rich phase and Cu atoms in Ag-rich phase) quickly exit the matrix and agglomerate into Cu grains and Ag grains, leading to the demixing and grain coarsening in the Cu-Ag layers (Fig. 5b).

The schematic diagrams in Fig. 7 compare and summarize the microstructure evolutions of the Cu/Fe and Cu-Ag/Fe multilayers upon annealing at different temperatures. In the low temperature regime ($T \leq 400$°C), the microstructure evolution in both systems is dominated by in-plane grain growth driven by the minimization of excess GB energy. Meanwhile, the layer interfaces remain intact with no discernable roughening. Annealing at 500°C and 600°C results in the massive increase of the grain size in the Cu/Fe multilayer as shown in the statistics in Fig. 6, indicating the accelerated lateral movement of column grain boundaries. The GB velocity (v) can be expressed as [65]:

$$v = M_{gb} \cdot \gamma_{gb} \cdot \kappa \tag{2}$$

where M_{gb} is the GB mobility, and κ is the local curvature. Therefore, the accelerated grain growth rate is tightly associated with the increasing boundary mobility as temperature increases. Compared with the Cu/Fe multilayer, the increase of grain size of Fe layers induced by annealing in the Cu-Ag/Fe multilayer is less dramatic, indicating the reduced GB mobility.

Annealing at 500°C also initiated the layer structure instability in Cu/Fe multilayer, manifested by the evident grooving at the

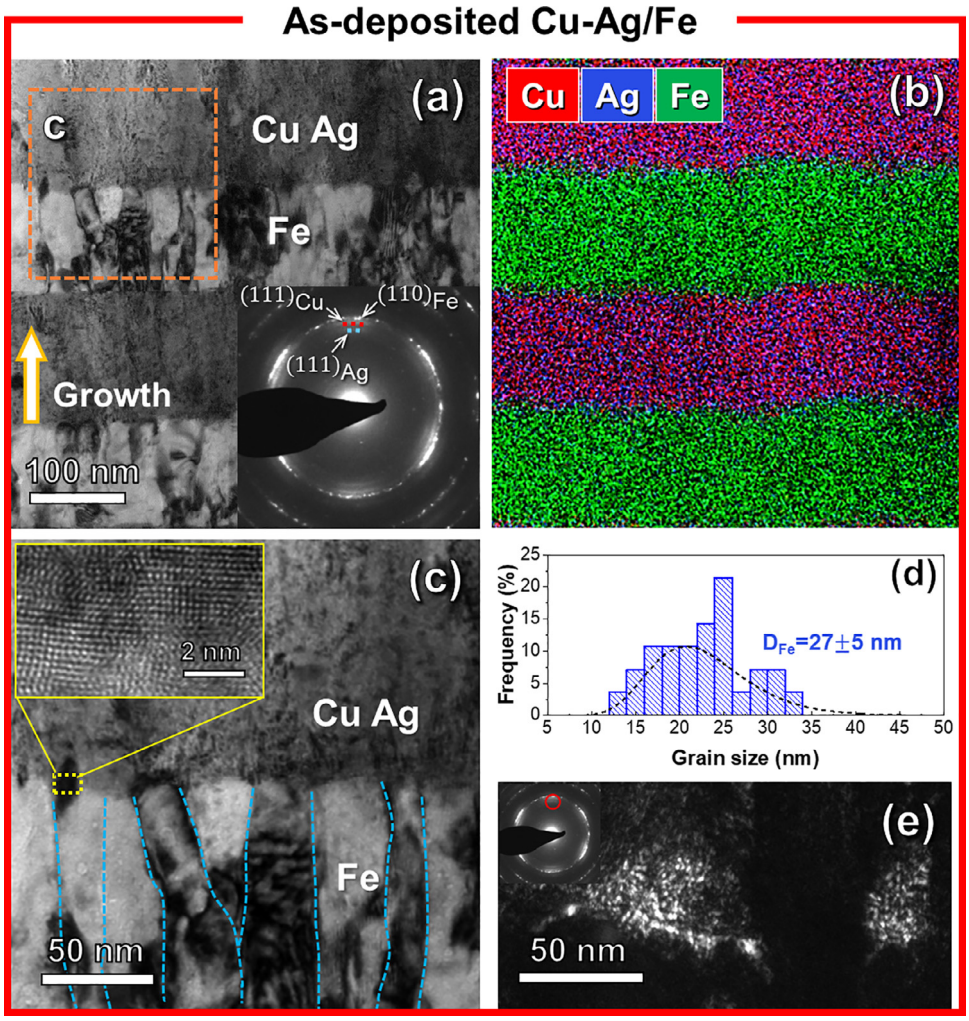

Fig. 2. Microstructures of as-deposited Cu-Ag/Fe 100 nm multilayer on SiO_2 substrate. (a) XTEM of Cu-Ag/Fe multilayer and the corresponding SAD pattern. (b) EDS map showing the elemental distributions. (c) Magnified TEM micrograph showing the columnar grains in Fe layers and the inserted HRTEM micrograph showing nanocrystalline grains in CuAg layers. (d) The statistical study showing that the average grain size of Fe is 27 nm. (e) Dark-field (DF) TEM image showing the substructure size in CuAg layer is less than 5 nm. The diffraction beam used for DF images is marked by the red circle.

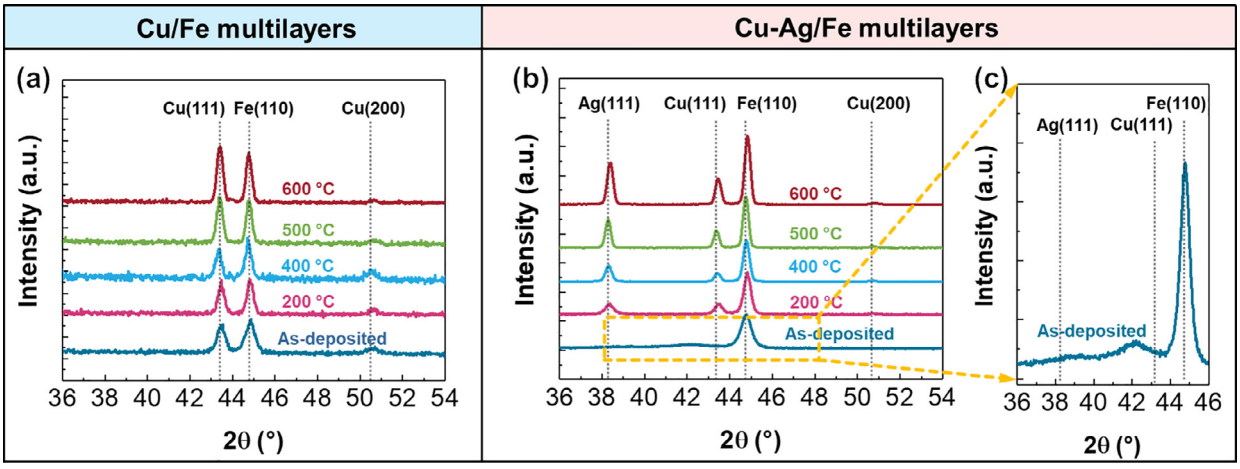

Fig. 3. (a-b) XRD patterns of Cu/Fe 100 nm and Cu-Ag/Fe 100 nm multilayers annealed up to 600°C. (c) Magnified XRD pattern of the as-deposited Cu-Ag/Fe 100 nm multilayer. The broad humps at 38°-40° and 41°-43° emerge due to the mixture of supersaturated Cu and Ag nanograins in the as-deposited films.

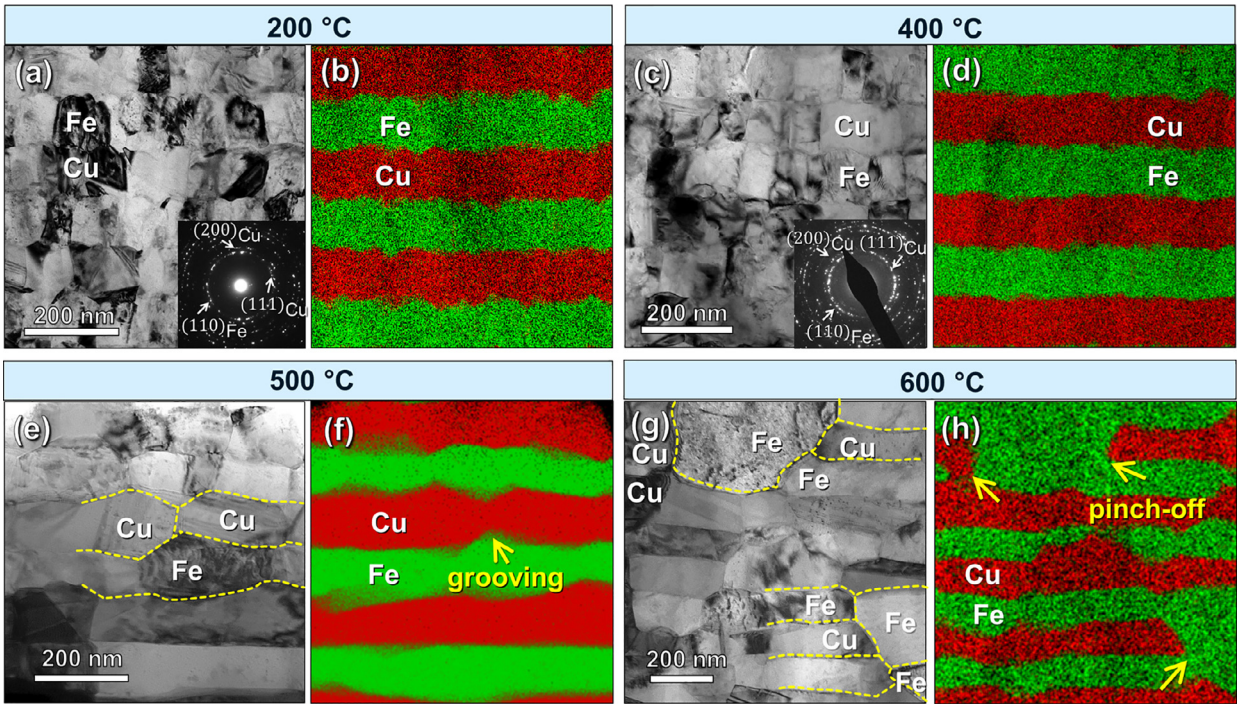

Fig. 4. XTEM micrographs and EDS maps showing the microstructure evolution of Cu/Fe 100 nm multilayer upon annealing at different temperatures. (a-b) 200°C. (c-d) The retention of flat and intact layer interfaces at 400°C. (e-f) Grooving and grain growth were observed after annealing at 500°C. (g-h) Layer pinch-off occurred after 600°C annealing.

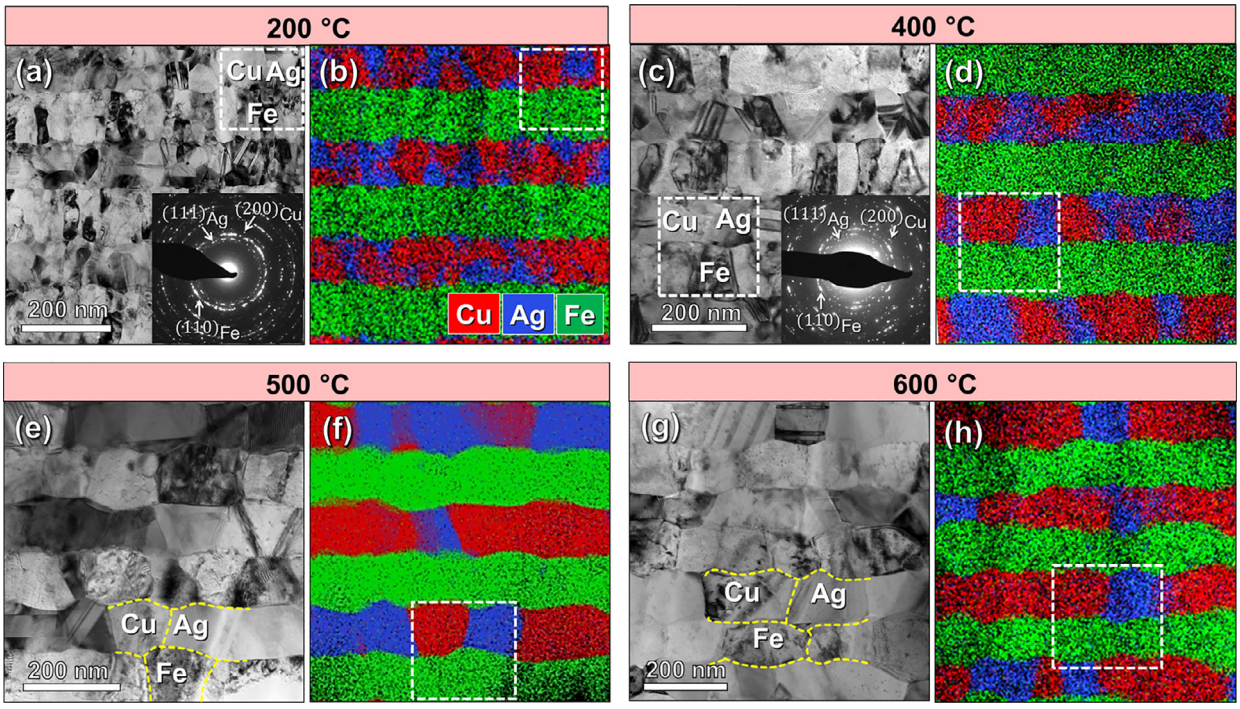

Fig. 5. XTEM micrographs and EDS maps showing the microstructure evolution of Cu-Ag/Fe 100 nm multilayer annealed up to 600°C. (a-b) Phase separation of Cu and Ag after annealing at 200°C. The white dashed boxes in a and b outline the region where Cu, Ag, Fe grains meet each other and form the triphase triple junction. (c-d) Microstructure of Cu-Ag/Fe multilayer annealed at 400°C. (e-f) The complete phase separation of Cu and Ag and insignificant layer interface roughening after 500°C annealing. (g-h) Layer interfaces remained stable upon 600°C annealing.

intersections between GBs and layer interfaces. The grooving development is favored at high temperature due to the accelerated diffusive mass transport. Further annealing at 600°C led to the complete layer disintegration as the groove depth exceeded the half layer thickness. In contrast, the grooves in Cu-Ag/Fe multilayer were less discernable with minor perturbations along layer interfaces after annealing at 500°C. Furthermore, the grooving at 600°C resulted in the wavy interface but no pinch-offs in the Cu-Ag/Fe multilayer.

4.2. GB Grooving kinetics

The development of GB grooving is a consequence of diffusive mass transport along the GBs and phase boundaries [66]. The pi-

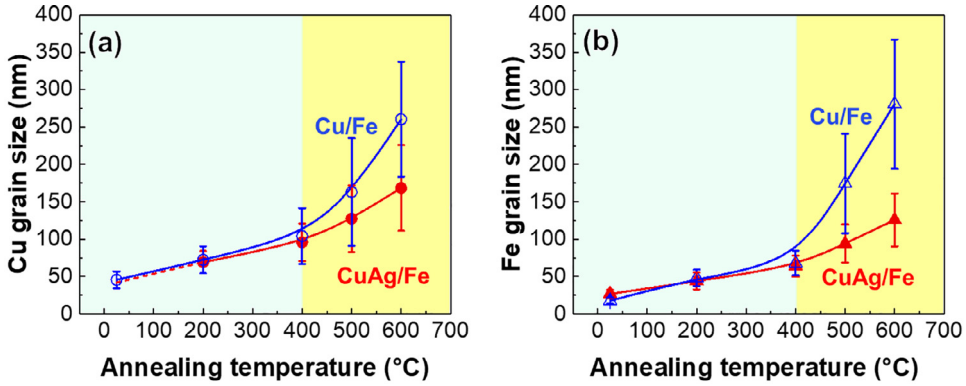

Fig. 6. Comparison of the grain size evolution of (a) Cu grains and (b) Fe grains in the Cu/Fe and Cu-Ag/Fe multilayers as a function of annealing temperature.

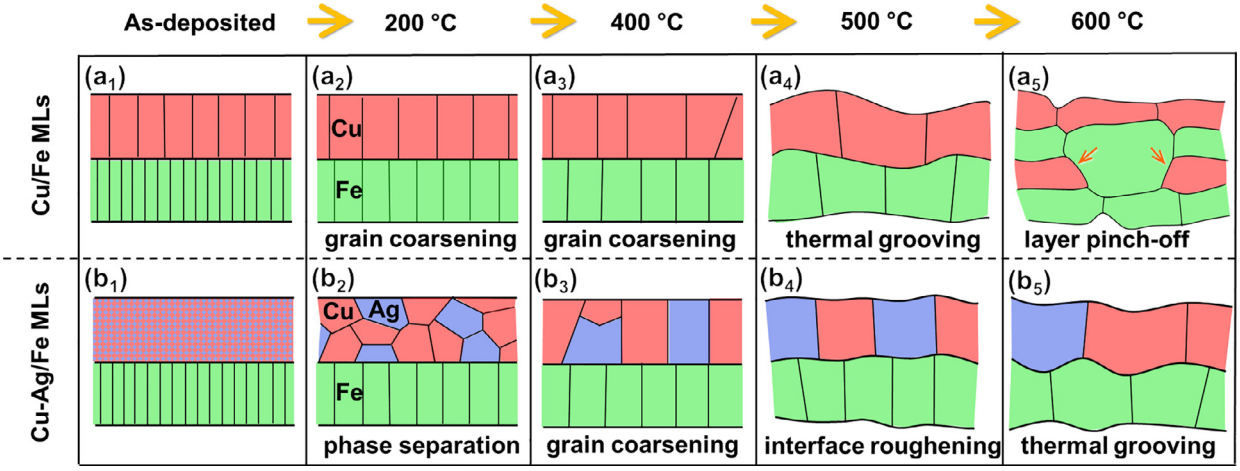

Fig. 7. Schematic illustration of the microstructure evolution of Cu/Fe and Cu-Ag/Fe multilayers annealed up to 600°C. The Fe grains are colored in green, Cu grains in red and Ag grains in blue.

oneering work by Mullins on free surface profile evolution during thermal grooving shows a $t^{1/4}$ dependence of grooving depth when surface diffusion is dominant over bulk transport, where t is time [67,68]. The model adopts a 2D geometry with local equilibrium groove angle and an assumption of isotropic interface energy. The analysis suggests the grooving kinetics is governed by the GB diffusivity and the ratio between GB energy and interface energy [67,68]. High temperature thus exacerbates grooving by accelerating diffusion. The grooving theory was further developed to predict the grooving kinetics in multilayers with immiscible components and polycrystalline structures [45,48,56,69]. The $t^{1/4}$ dependence is tenable even when considering anisotropic surface energy and relaxing the small slope approximation [70–72]. These credible models define the foundation to estimate the time dependent evolution of grooving profiles for both Cu/Fe and Cu-Ag/Fe multilayers during annealing. Since high temperature promotes the pinch-off of layer structure by accelerated grooving development, we will focus on the discussion of grooving kinetics at 600°C and compare the structure stability between the Cu/Fe and Cu-Ag/Fe multilayers. The analysis is based on the isotropic interface energy assumption. Meanwhile, it should be noticed that even though the predicted $t^{1/4}$ dependence of grooving development is in agreement with both theoretical extensions of original Mullins' model on polycrystalline multilayers [48,66,69,73] and experimental observations [74], the $t^{1/4}$ dependence may become invalid when the groove width becomes so large that the two adjacent grooves start to interact with each other [48,69,75]. Therefore, calculation based on the Mullins model serves to compare the grooving kinetics and relative interface mobility, but may not accurately predict the pinch-off time as will be discussed later.

Wang et al. improved the grooving model and considered the restrictions imposed by the mechanical coupling between different phases to avoid internal void formation at the phase boundaries [48]. The migration of interphase boundary stems from the chemical potential gradient along the boundary. Assuming the volume conservation, the time dependent grooving development can be expressed as [48]:

$$h_g = 0.77 \cot\theta_{eq.} \left(\gamma_{PB} \cdot M_{PB} \cdot t\right)^{\frac{1}{4}} \tag{3}$$

where h_g is the grooving depth, $\theta_{eq.}$ represents the one-half of equilibrium grooving angle, γ_{PB} is the phase boundary energy, and M_{PB} is the mobility of phase boundary. M_{PB} is determined by the interdiffusion of atoms (assuming a and b species) along the phase boundary and can be estimated as [48]:

$$M_{PB} = \frac{\delta_{PB}}{2kT} \frac{D^a_{PB}\Omega^a D^b_{PB}\Omega^b}{\left(D^a_{PB}\Omega^a + D^b_{PB}\Omega^b\right)} \tag{4}$$

where δ_{PB} represents the thickness of phase boundaries and is normally taken as 5×10^{-10} m, k is the Boltzmann's constant, T is the absolute temperature, D^a_{PB} and D^b_{PB} correspond to the diffusivity of a and b species along the phase boundaries, and Ω^a and Ω^b are the atomic volume of a and b species respectively. Previous study on the stability of Cu/Ag multilayer suggests the diffusivity along phase boundaries can be approximated by GB diffusivity [76]. Therefore, the phase boundary diffusivities in our analysis were estimated by using the diffusivities along their respective

Table 1
Grain size evolution in Cu/Fe and Cu-Ag/Fe multilayers after annealing up to 600°C.

Annealing temperature	Cu/Fe multilayer		Cu-Ag/Fe multilayer	
	Fe grains (nm)	Cu grains (nm)	Fe grains (nm)	Cu grains (nm)
As-deposited (RT)	18 ± 4	45 ± 12	27 ± 5	-
200°C	48 ± 11	72 ± 18	44 ± 11	69 ± 15
400°C	68 ± 17	104 ± 38	64 ± 17	96 ± 25
500°C	175 ± 67	163 ± 72	94 ± 26	127 ± 45
600°C	281 ± 86	260 ± 77	126 ± 36	169 ± 58

Table 2
Materials parameters at 600°C for calculation.

	GB energy ($J{\cdot}m^{-2}$)	GB diffusivity ($m^2{\cdot}s^{-1}$)	Atomic volume (10^{-29} m^3)
Cu	0.63 [62]	1.10×10^{-11}	1.182
Fe	0.86 [39]	2.17×10^{-13}	1.179
Ag	0.56 [39]	2.63×10^{-11}	1.790

Table 3
Materials parameters at 600°C for calculation.

	Interface energy ($J{\cdot}m^{-2}$)	Interface mobility($m^4{\cdot}J^{-1}{\cdot}s^{-1}$)
Cu/Fe	0.52 [81]	5.41×10^{-32}
Ag/Fe	0.99 [82]	1.04×10^{-31}
Cu/Ag	0.57 [74]	-

GBs. For bcc Fe, the GB diffusivity at 600 °C (below Curie temperature) was estimated by [77]:

$$D_{gb} = D_{gb}^0 \cdot \exp\left(-\frac{Q_{gb}}{RT}\right) \quad (5)$$

where D_{gb} is the grain boundary diffusion coefficient, D_{gb}^0 is the frequency factor and is estimated to be 2.24×10^{-4} m^2/s (assuming grain boundary thickness δ is 5×10^{-10} m) [77]. Q_{gb} is the activation energy for grain boundary diffusion and is taken as 4.15×10^4 cal/mol (1.74×10^5 J/mol) [77]. The calculation yields a D_{gb} of ~2.17×10^{-13} m^2/s. This value is comparable to the D_{gb} of bcc Fe at similar temperature in previous studies [77,78].

D_{gb}^0 of Cu is estimated to be 2.0×10^{-5} m^2/s, and Q_{gb} is 2.50×10^4 cal/mol (1.05×10^5 J/mol) [79]. $D_{gb}$of Cu at 600 °C is calculated to be ~1.10×10^{-11} m^2/s. For Ag, D_{gb}^0 is 3.0×10^{-6} m^2/s, Q_{gb} is 2.02×10^4 cal/mol (8.45×10^4 J/mol) [80], and $D_{gb}$of Ag at 600 °C is calculated to be ~2.63×10^{-11} m^2/s. The interface energy is taken as 0.52 $J{\cdot}m^{-2}$ for Cu/Fe interface (assuming incoherent) [81], 0.99 $J{\cdot}m^{-2}$ for Ag/Fe interface [82], and 0.57 $J{\cdot}m^{-2}$ for Cu/Ag interface [74]. The material parameters including the interface energy, GB diffusivity (at 600°C), and atomic volume of Cu, Ag and Fe are tabulated in Table 2 and Table 3. It is worth mentioning that since the groove development is highly dependent on the interface energy and $\theta_{eq.}$, the variation of local crystal orientation and interface energy may lead to different grooving depth and asymmetric grooving shape as seen in the annealed Cu/Fe and Cu-Ag/Fe multilayers.

The value of $\theta_{eq.}$ is closely associated with the ratio between GB energy and interphase boundary energy as well as the multilayer morphologies [66]. The grain morphologies of multilayers can be categorized into two typical scenarios, i.e. staggered morphology and aligned morphology. For the staggered morphology, the columnar GBs in the alternating layers are laterally offset by as much as half of the grain size as shown in Fig. 8a. In contrast, the aligned morphology refers to the cases where columnar GBs in adjacent layers are coincident as shown in Fig. 8b. For the staggered morphology shown in Fig. 8a, the $\theta_{eq.}$ was determined by balancing the GB energy with the projection of phase boundary energy along the vertical direction at triple junctions. In contrast, the $\theta_{eq.}$ for aligned structure was derived by the interfacial tension balance at the quadruple junction as shown in Fig. 8b. The $\theta_{eq.}$ for the two (staggered vs aligned) structures can be calculated as [48]:

$$2\gamma_{PB} \cdot cos\theta_{eq.} = \gamma_{gb,b} \text{ (staggered)} \quad (6)$$

$$2\gamma_{PB} \cdot cos\theta_{eq.} = \gamma_{gb,b} - \gamma_{gb,a} \text{ (aligned)} \quad (7)$$

Here $\gamma_{gb,b}$ corresponds to the element with a larger GB energy, i.e. Fe in Cu/Fe multilayer. As can be seen from Eq. 5, part of the GB energy of Fe is balanced by the coincident Cu GB, leading to the reduction of driving force for grooving at the junctions. Consequently, the aligned morphology is expected to exhibit less grooving development and higher stability than the staggered structure. Both the aligned and staggered structure were considered when calculating the groove depth development in Fe layers in Cu/Fe multilayer. The $\theta_{eq.}$ is estimated to be 34.2° for the staggered morphology, and 77.2° for the aligned structure, indicating that the aligned structure is morphologically more stable. The model prediction shown in Fig. 8c compares the time dependent groove depth evolution in Fe layers for the two configurations. The grooving develops much more rapidly in the staggered morphology than in the aligned structure. Wan et al. contend that the pinch-off time is closely related to the layer morphology and the distance between two neighboring triple junctions [45]. The staggered and aligned morphology stand for two extreme cases of multilayer structure and set up the upper and lower bounds of grooving depth development, which outline the green shadowed region in Fig. 8c.

Next, we attempt to estimate the grooving dynamics of the Cu layers in Cu-Ag/Fe multilayer. The addition of Ag in Cu layers leads to the formation of Cu-Ag-Fe immiscible triphase triple junction as shown in Fig. 9b. The equilibrium dihedral angle can be estimated by [83]:

$$\frac{\gamma_{Cu/Fe}}{\sin 2\theta_1} = \frac{\gamma_{Ag/Fe}}{\sin 2\theta_2} = \frac{\gamma_{Cu/Ag}}{\sin 2\theta_3} \quad (8)$$

where

$$2\theta_1 + 2\theta_2 + 2\theta_3 = 2\pi \quad (9)$$

Further simplification and calculation yield,

$$\cos 2\theta_3 = \frac{\gamma_{Cu/Ag}^2 - \gamma_{Cu/Fe}^2 - \gamma_{Ag/Fe}^2}{2\gamma_{Cu/Fe} \cdot \gamma_{Ag/Fe}} \quad (10)$$

Therefore, the half of equilibrium grooving angle, θ_3, at the triphase triple junction is calculated to be 77.0°. The larger $\theta_{eq.}$ comparing to that in Cu/Fe multilayer (34.2°) is associated with the reduced driving force for groove development resulted from the comparatively large value of Ag/Fe interface energy. The layer interface in Cu-Ag/Fe multilayer consists of alternating Cu/Fe interface and Ag/Fe interface. The mathematic description of such complex interface movement and mobility remains challenging and needs further investigation. To estimate the grooving kinetics in

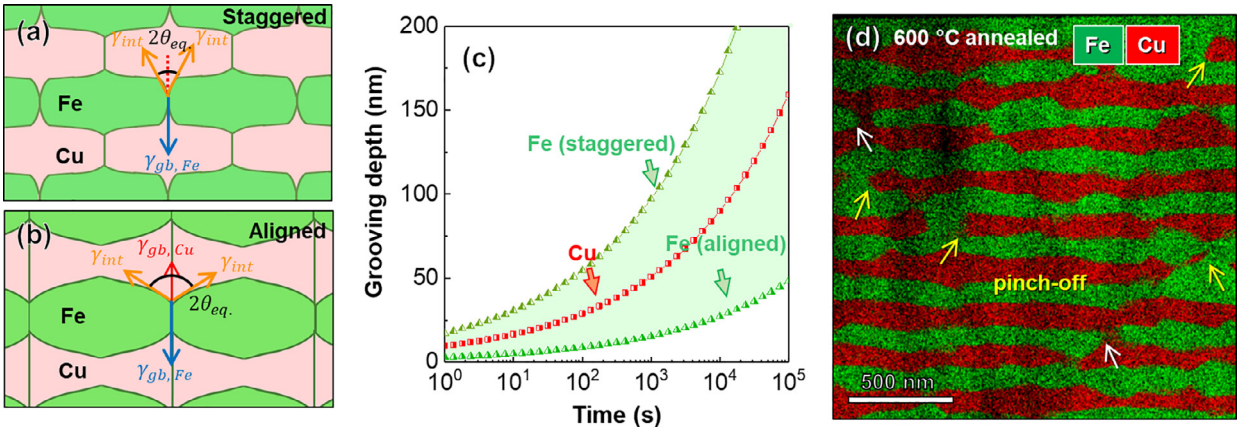

Fig. 8. (a-b) Schematics illustrating the staggered structure in polycrystalline Cu/Fe 100 nm multilayers where the grain boundaries in alternating layers are laterally offset, and the aligned morphologies where the columnar boundaries in adjacent layers are aligned. (c) Calculated grooving depth as a function of time at 600°C for Fe layers (including the aligned and staggered morphologies) and Cu layers. (d) EDS map of Cu/Fe multilayer annealed at 600°C showing the pinch-off of layer structure in both Cu layers (labeled by yellow arrows) and Fe layers (indicated by white arrows).

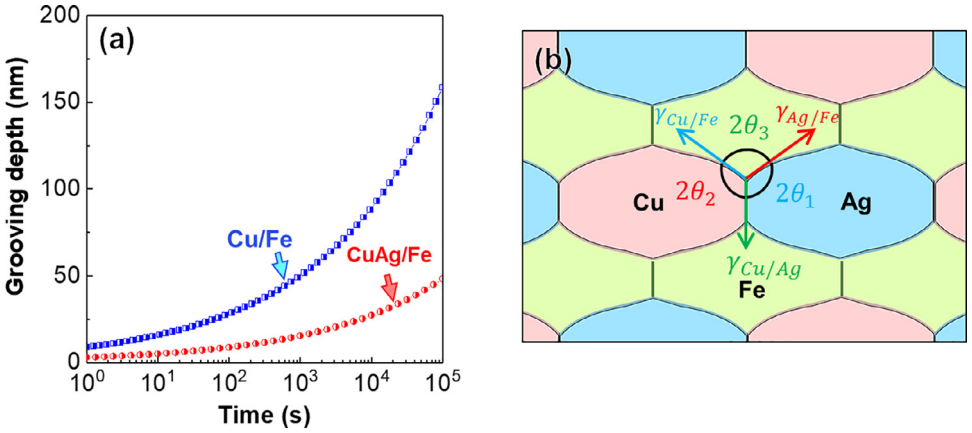

Fig. 9. (a) Comparison of the grooving development in Cu of Cu/Fe multilayers and CuAg in Cu-Ag/Fe multilayers at 600°C. (b) Schematic diagram showing the balance of phase boundary tensions at the triphase triple junction.

Cu-Ag/Fe multilayer, we approximate the mobility of the layer interface with the Cu/Fe interface. Nevertheless, it should be noticed that the movement of layer interface and subsequent groove development requires the coordinated motion of triple junctions. Prior studies show that excessive grooving may form at triple junctions when compared to GBs [84,85]. Such accelerated grooving can be attributed to the higher diffusion fluxes and higher line energy of triple junctions (exceeding GB energy) [84]. Given the effect of thermal grooving on retarding the GB motion as previously demonstrated by Mullins and Frost et al. [60,61], the influence of triphase triple junctions on the mobility of layer interfaces and column boundaries warrants further exploration. Fig. 9a compares the grooving kinetics of Cu-Ag/Fe and Cu/Fe multilayers calculated based on Mullins model.

The foregoing discussion on grooving kinetics assumes the development of grooves arises from the diffusion along layer interfaces alone and does not involve mass transport along columnar GBs. It is worth mentioning that the diffusion along the columnar GBs could result in exacerbated grooving [86–88]. Schematics illustrating the combined diffusion along layer interfaces as well as along GBs in Cu-Ag/Fe multilayer is shown in Fig. S1a-b. In contrast to the Mullins type of groove shape, Vogel et al. observed deep, channel-like grooves in Al bicrystal/In-Al melt after elevated temperature annealing as a result of GB diffusion [88]. Such instabilities of GB grooves could be aggravated as GB diffusion accelerates [88]. A similar accelerated groove deepening phenomenon was observed when applying tensile stress normal to the planar GBs [87]. Moreover, Amram et al. discovered the unusually flat, ridgeless GB grooves in an annealed bicrystal Ni films deposited on sapphire substrates [86]. It was shown that GB grooves could deepen much faster with the concurrent surface, GB and interface diffusion than with surface diffusion alone [86]. They evaluated the effect of GB diffusion on grooving development by using [86]:

$$h_g' = 1.708 \cot\theta_{eq.} (\gamma_{PB} \cdot M_{PB} \cdot t)^{\frac{1}{4}} \tag{11}$$

where h_g' is the modified grooving depth after considering GB diffusion. A comparison of the modified Cu grooving depth in Cu/Fe and Cu-Ag/Fe with the ones calculated using classical Mullins model is shown in Fig. S1c. The modified model predicts that GB grooving depth is about two times as much as that predicted by the Mullins model.

As discussed earlier, the $t^{1/4}$ dependence may become invalid when the two adjacent grooves start to interact with each other [48,69,75]. The effects of finite grain size were found to introduce a time scale $t \sim d^4$ (d is the grain size), beyond which the $t^{1/4}$dependence decays to a steady-state value. According to Wan et al., the critical time ($t_{crit.}$) at which $t^{1/4}$dependence may become invalid can be estimated via [45,48]:

$$t_{crit.} \approx \left(\frac{s}{\pi}\right)^4 \frac{1}{M_{PB} \cdot \gamma_{PB}} \tag{12}$$

where s is the separation distance between two maxima of the groove profile and can be taken as half of the grain size in a stag-

gered morphology. Consequently, the corresponding critical grain size ($d_{crit.}$) below which the $t^{1/4}$dependence is unlikely to hold can be expressed as [45]:

$$d_{crit.} = 2s \approx 4h \cdot \tan\theta_{eq.} \tag{13}$$

where h is the layer thickness and $\theta_{eq.}$ is the equilibrium dihedral angle. Given that the layer thickness in the current study is 100 nm, $d_{crit.}$ of Cu layers is estimated to be 1733 nm in Cu-Ag/Fe multilayer and 304 nm in Cu/Fe multilayer. Comparing with the measured average Cu grain sizes, it is likely that the grooving depth predicted from Mullins theory is overestimated. Therefore, the Mullins model can be applied to compare the grooving kinetics of multilayer systems with different chemistry and different microstructure (aligned vs. staggered), which may provide guidelines on designing stable layer structure by tuning the interface/GB energy and layer morphology. However, precautions need to be taken to evaluate the reliability of these model in predicting the precise layer pinch-off time.

4.3. Enhanced thermal stability in triphase Cu-Ag/Fe multilayer

Fig. 6a reveals the substantial difference of Cu grain size between Cu/Fe and Cu-Ag/Fe multilayers after annealing. With an effort on constructing the pinch-off maps for polycrystalline multilayers, a stability criteria considering the aspect ratio h/d and the equilibrium dihedral angles was derived [48,56]. In general, pinch-off of Fe layers will not occur if [48]:

$$\frac{h}{d} > \begin{cases} \frac{\cot\theta_{eq.}}{3} \ (aligned) \\ \frac{\cot\theta_{eq.,\ Cu} + 2\cot\theta_{eq.,Fe}}{6} \ (staggered) \end{cases} \tag{14}$$

The critical aspect ratio is estimated to be 0.08 for aligned morphology, and the corresponding maximum Fe grain size is 1320 nm for multilayers with 100 nm layer thickness to avoid layer structure breakdown. For the staggered structure, the critical aspect ratio is calculated to be 0.62, corresponding to a grain size of 160 nm to maintain the structure integrity. Comparing with the measured average Fe grain size, the layer structure of Cu-Ag/Fe multilayer is expected to remain intact after 600 °C annealing while Cu/Fe may suffer from pinch-off. This prediction matches well with our experimental observations. The above analysis suggests that the coarsening of grains would impair the layer structure stability. The comparatively smaller grain size in Cu-Ag/Fe multilayer may therefore enhance its resistance to layer structure breakdown.

Next, we attempt to interpret the much smaller Cu and Fe grain sizes in Cu-Ag/Fe multilayer than the annealed Cu/Fe multilayer. The suppression of grain coarsening of Cu grains in the Cu-Ag/Fe multilayer may be tightly associated with the non-conservative motion of Cu/Ag interfaces that requires the long-range diffusional fluxes of Cu atoms. For Cu grains in Cu/Fe multilayer, there is no composition difference across the interfaces of adjoining grains, and the migration of interfaces/GBs occurs in the absence of a diffusion flux [89,90]. This type of interface movement can be categorized as conservative interface motion and only requires local atom transport across the interface such as atom shuffling [90]. In comparison, the motion of Cu/Ag interface in Cu-Ag/Fe multilayer has to be coupled with the long-range diffusion of Cu (or Ag) atoms from the next-nearest Cu (or Ag) neighbors [90]. The diffusion distance of such process is comparable to the grain size. Comparing to the conservative motion that only demands a diffusion distance of interatomic spacing, such difference could result in the large disparity of interface mobilities, which may lead to the more sluggish lateral boundary migration and consequently smaller Cu grain size.

Surprisingly, even though the restrictions imposed by immiscible second phase boundaries are absent in Fe layers, the Fe column size in Cu-Ag/Fe multilayer is still much smaller than that in the Cu/Fe multilayer after annealing at 500°C and 600°C (Fig. 6b). To interpret the origin of such drastic difference of Fe grain size between Cu/Fe and Cu-Ag/Fe multilayers, it is worth noting the substantial impact of multilayer morphology on layer structure stability. Wan *et al.* reported that the stability of multilayers with different morphologies was tightly associated with the relative distance between the two neighboring triple junctions along the layer interface [45]. In general, it was expected that the stability of layered structure would increase with the decreasing triple junction distance, and the optimum thermal stability was achieved through the aligned morphology [45]. The improved thermal stability of the aligned morphology derives from the reduced driving force for groove development at quadruple points. Previous study by Misra et al. show that the formation of the aligned morphology is favored by the removal of high energy interface segment [55]. Once Fe columnar GBs arrive at the quadruple point and form the aligned morphology, it becomes difficult for the Fe GBs to break away from such a stable structure. Hence, the quadruple points at the aligned morphologies trap Fe GBs and lead to the stagnation of lateral GBs in Fe layers. Fig. S2 highlights the aligned morphology in both Cu/Fe and Cu-Ag/Fe multilayers after 600°C annealing. Compared with the Cu/Fe multilayer, the much smaller Cu and Ag grains in Cu-Ag/Fe multilayer provide more trapping sites to arrest the movement of Fe GBs, thus resulting in the smaller Fe grain size after annealing. Meanwhile, the small columnar grain size may also promote the formation of aligned grain morphology, which is beneficial to slow down the groove development. It is interesting to note that both aligned and staggered morphologies were frequently observed in Cu-Ag/Fe multilayer. One possibility that may lead to the coexistence of both aligned and staggered morphology in Cu-Ag/Fe multilayer is that the grooving development may also help to stagnate or terminate the GB movement and effectively anchor the nanostructures [48,60,74]. It was reported that GBs can be anchored to the grooves due to the lack of necessary curvature for GBs to break free [74], which may in turn affect the microstructure after annealing.

In summary, the improved thermal stability of Cu-Ag/Fe multilayer due to the construction of triphase triple junction or the introduction of the immiscible second phase (Ag) into Cu layers can be understood from both kinetics and thermodynamics point of view. Kinetically, the Cu/Ag phase boundaries have much lower mobility comparing to Cu GBs. This could benefit the structure integrity in two folds. Firstly, according to the grain aspect ratio criterion, the smaller grain size gives rise to higher structure stability of multilayers. Secondly, the smaller grain size also provides more trapping sites to arrest the moving Fe GBs, therefore forming the preferred aligned structure. From the thermodynamics perspective, the larger θ(eq.) (77°) at Cu-Ag-Fe triple junctions comparing to that in Cu/Fe multilayer (34.2°) reduces the driving force for groove development. The comparatively larger value of Ag/Fe interface energy than the Cu/Fe interface energy can compensate more of the Fe GB energy and thus lower the driving force for grooving.

5. Conclusions

In this study, we report the enhanced thermal stability of Cu-Ag/Fe multilayer with immiscible triphase triple junction comparing to Cu/Fe multilayers. Several major differences were observed regarding the microstructure evolution of Cu-Ag/Fe and Cu/Fe multilayers. In low temperature regime, in-plane grain coarsening prevails in both systems. Annealing at 500°C induces prominent thermal grooving and rapid in-plane grain growth in Cu/Fe multilayer. Further increase of annealing temperature to 600°C leads to the complete breakdown of layer structure and spheroidization of the discontinuous layers in Cu/Fe multilayer. In comparison, the layer structures of Cu-Ag/Fe multilayer remained stable up to 600°C

with minor perturbations along layer interfaces and insignificant in-plane grain coarsening. The roles of Cu-Ag-Fe triphase triple junction on impeding boundary migration as well as the grooving kinetics are discussed to interpret the excellent thermal stability of Cu-Ag/Fe multilayer comparing to Cu/Fe multilayer. This study provides a feasible approach to design thermally stable nanostructured multilayers, and opens up new possibilities of using immiscible triphase triple junctions to impede thermal grooving and layer pinch-offs.

Declaration of Competing Interest

The authors declare that they have no known competing financial interests or personal relationships that could have appeared to influence the work reported in this paper.

Acknowledgment

We acknowledge financial support by NSF-CMMI-MOM 1728419. H. Wang acknowledges the support from the U.S. Office of Naval Research (N00014-20-1-2043). Access to the Life Sciences Microscopy Center and Materials Science Microscopy Center at Purdue University are also acknowledged.

Supplementary materials

Supplementary material associated with this article can be found, in the online version, at doi:10.1016/j.actamat.2021.116679.

References

[1] Y.H. Zhao, X.Z. Liao, S. Cheng, E. Ma, Y.T. Zhu, Simultaneously increasing the ductility and strength of nanostructured alloys, Adv. Mater. 18 (2006) 2280–2283.
[2] T. Zhu, J. Li, Ultra-strength materials, Prog. Mater Sci. 55 (2010) 710–757.
[3] I.A. Ovid'ko, R.Z. Valiev, Y.T. Zhu, Review on superior strength and enhanced ductility of metallic nanomaterials, Prog. Mater Sci. 94 (2018) 462–540.
[4] Q. Li, S. Xue, J. Wang, S. Shao, A.H. Kwong, A. Giwa, Z. Fan, Y. Liu, Z. Qi, J. Ding, H. Wang, J.R. Greer, H. Wang, X. Zhang, High-strength nanotwinned Al alloys with 9R phase, Adv. Mater. 30 (2018) 1704629.
[5] X. Zhang, A. Misra, H. Wang, T.D. Shen, M. Nastasi, T.E. Mitchell, J.P. Hirth, R.G. Hoagland, J.D. Embury, Enhanced hardening in Cu/330 stainless steel multilayers by nanoscale twinning, Acta Mater. 52 (2004) 995–1002.
[6] Y.F. Zhang, S. Xue, Q. Li, J. Li, J. Ding, T.J. Niu, R. Su, H. Wang, X. Zhang, Size dependent strengthening in high strength nanotwinned Al/Ti multilayers, Acta Mater. 175 (2019) 466–476.
[7] J. Wang, A. Misra, An overview of interface-dominated deformation mechanisms in metallic multilayers, Curr. Opin. Solid State Mater. Sci. 15 (2011) 20–28.
[8] N.A. Mara, D. Bhattacharyya, P. Dickerson, R.G. Hoagland, A. Misra, Deformability of ultrahigh strength 5nm Cu/Nb nanolayered composites, Appl. Phys. Lett. 92 (2008) 231901.
[9] R. Su, D. Neffati, Q. Li, S. Xue, J. Cho, J. Li, J. Ding, Y. Zhang, C. Fan, H. Wang, Y. Kulkarni, X. Zhang, Ultra-high strength and plasticity mediated by partial dislocations and defect networks: part I: texture effect, Acta Mater. 185 (2020) 181–192.
[10] A. Misra, X. Zhang, D. Hammon, R.G. Hoagland, Work hardening in rolled nanolayered metallic composites, Acta Mater. 53 (2005) 221–226.
[11] T.J. Rupert, C.A. Schuh, Sliding wear of nanocrystalline Ni–W: structural evolution and the apparent breakdown of Archard scaling, Acta Mater. 58 (2010) 4137–4148.
[12] H.A. Padilla, B.L. Boyce, C.C. Battaile, S.V Prasad, Frictional performance and near-surface evolution of nanocrystalline Ni–Fe as governed by contact stress and sliding velocity, Wear 297 (2013) 860–871.
[13] X. Chen, Z. Han, X. Li, K. Lu, Lowering coefficient of friction in Cu alloys with stable gradient nanostructures, Sci. Adv. 2 (2016) e1601942.
[14] T.J. Rupert, W. Cai, C.A. Schuh, Abrasive wear response of nanocrystalline Ni–W alloys across the Hall–Petchbreakdown, Wear 298–299 (2013) 120–126.
[15] N. Li, E.G. Fu, H. Wang, J.J. Carter, L. Shao, S.A. Maloy, A. Misra, X. Zhang, He ion irradiation damage in Fe/W nanolayer films, J. Nucl. Mater. 389 (2009) 233–238.
[16] E.G. Fu, A. Misra, H. Wang, L. Shao, X. Zhang, Interface enabled defects reduction in helium ion irradiated Cu/V nanolayers, J. Nucl. Mater. 407 (2010) 178–188.
[17] I.J. Beyerlein, A. Caro, M.J. Demkowicz, N.A. Mara, A. Misra, B.P. Uberuaga, Radiation damage tolerant nanomaterials, Mater. Today 16 (2013) 443–449.
[18] X. Zhang, N. Li, O. Anderoglu, H. Wang, J.G. Swadener, T. Höchbauer, A. Misra, R.G. Hoagland, Nanostructured Cu/Nb multilayers subjected to helium ion-irradiation, Nucl. Instrum. Methods Phys. Res. Sect. B 261 (2007) 1129–1132.
[19] A. Misra, M.J. Demkowicz, X. Zhang, R.G. Hoagland, The radiation damage tolerance of ultra-high strength nanolayered composites, JOM 59 (2007) 62–65.
[20] M. Ames, J. Markmann, R. Karos, A. Michels, A. Tschöpe, R. Birringer, Unraveling the nature of room temperature grain growth in nanocrystalline materials, Acta Mater. 56 (2008) 4255–4266.
[21] H. Gleiter, Nanostructured materials: basic concepts and microstructure, Acta Mater. 48 (2000) 1–29, doi:10.1016/S1359-6454(99)00285-2.
[22] T. Chookajorn, H.A. Murdoch, C.A. Schuh, Design of stable nanocrystalline alloys, Science 337 (2012) 951 LP – 954.
[23] H. Gleiter, Nanocrystalline materials, Prog. Mater Sci. 33 (1989) 223–315.
[24] G. Sharma, J. Varshney, A.C. Bidaye, J.K. Chakravartty, Grain growth characteristics and its effect on deformation behavior in nanocrystalline Ni, Mater. Sci. Eng. 539 (2012) 324–329.
[25] P.R. Cantwell, M. Tang, S.J. Dillon, J. Luo, G.S. Rohrer, M.P. Harmer, Grain boundary complexions, Acta Mater. 62 (2014) 1–48.
[26] D. Raabe, M. Herbig, S. Sandlöbes, Y. Li, D. Tytko, M. Kuzmina, D. Ponge, P.-P. Choi, Grain boundary segregation engineering in metallic alloys: a pathway to the design of interfaces, Curr. Opin. Solid State Mater. Sci. 18 (2014) 253–261.
[27] K. Boylan, D. Ostrander, U. Erb, G. Palumbo, K.T. Aust, An in-situ tem study of the thermal stability of nanocrystalline NiP, Scr. Metall. Mater. 25 (1991) 2711–2716.
[28] C.C. Koch, R.O. Scattergood, M. Saber, H. Kotan, High temperature stabilization of nanocrystalline grain size: thermodynamic versus kinetic strategies, J. Mater. Res. 28 (2013) 1785–1791.
[29] T. Roland, D. Retraint, K. Lu, J. Lu, Enhanced mechanical behavior of a nanocrystallised stainless steel and its thermal stability, Mater. Sci. Eng. 445–446 (2007) 281–288.
[30] E. Nes, N. Ryum, O. Hunderi, On the Zener drag, Acta Metall. 33 (1985) 11–22.
[31] D. Amram, C.A. Schuh, Interplay between thermodynamic and kinetic stabilization mechanisms in nanocrystalline Fe-Mg alloys, Acta Mater. 144 (2018) 447–458.
[32] Y.F. Zhang, R. Su, D.Y. Xie, T.J. Niu, S. Xue, Q. Li, Z. Shang, J. Ding, N.A. Richter, J. Wang, H. Wang, X. Zhang, Design of super-strong and thermally stable nanotwinned Al alloys via solute synergy, Nanoscale 12 (2020).
[33] T. Chookajorn, C.A. Schuh, Nanoscale segregation behavior and high-temperature stability of nanocrystalline W–20at.% Ti, Acta Mater. 73 (2014) 128–138.
[34] H.A. Murdoch, C.A. Schuh, Stability of binary nanocrystalline alloys against grain growth and phase separation, Acta Mater. 61 (2013) 2121–2132.
[35] R. Kirchheim, Grain coarsening inhibited by solute segregation, Acta Mater. 50 (2002) 413–419.
[36] J.W. Cahn, The impurity-drag effect in grain boundary motion, Acta Metall. 10 (1962) 789–798.
[37] Z. Fan, J. Jian, Y. Liu, Y. Chen, M. Song, L. Jiao, H. Wang, X. Zhang, situ studies on superior thermal stability of bulk FeZr nanocomposites, Acta Mater. 101 (2015) 125–135.
[38] T.H. Courtney, J.C.M. Kampe, Shape instabilities of plate-like structures—II. Analysis, Acta Metall. 37 (1989) 1747–1758.
[39] A.C. Lewis, D. Josell, T.P. Weihs, Stability in thin film multilayers and microlaminates: the role of free energy, structure, and orientation at interfaces and grain boundaries, Scr. Mater. 48 (2003) 1079–1085.
[40] D. Josell, F. Spaepen, Determination of the interfacial tension by zero creep experiments on multilayers—II. Experiment, Acta Metall. Mater. 41 (1993) 3017–3027.
[41] Y.F. Zhang, Q. Li, M. Gong, S. Xue, J. Ding, J. Li, J. Cho, T. Niu, R. Su, N.A. Richter, H. Wang, J. Wang, X. Zhang, Deformation behavior and phase transformation of nanotwinned Al/Ti multilayers, Appl. Surf. Sci. 527 (2020).
[42] Y.F. Zhang, R. Su, T.J. Niu, N.A. Richter, S. Xue, Q. Li, J. Ding, B. Yang, H. Wang, X. Zhang, Thermal stability and deformability of annealed nanotwinned Al/Ti multilayers, Scr. Mater. 186 (2020).
[43] R.L. Schoeppner, A.A. Taylor, M.J. Cordill, H.M. Zbib, J. Michler, D.F. Bahr, Precipitate strengthening and thermal stability in three component metallic nanolaminate thin films, Mater. Sci. Eng. 712 (2018) 485–492.
[44] Y. Kuru, M. Wohlschlögel, U. Welzel, E.J. Mittemeijer, Interdiffusion and stress development in Cu–Pd thin film diffusion couples, Thin Solid Films 516 (2008) 7615–7626.
[45] H. Wan, Y. Shen, J. Wang, Z. Shen, X. Jin, A predictive model for microstructure evolution in metallic multilayers with immiscible constituents, Acta Mater. 60 (2012) 6869–6881.
[46] H. Wan, Y. Shen, X. He, J. Wang, Modeling of microstructure evolution in metallic multilayers with immiscible constituents, JOM 65 (2013) 443–449, doi:10.1007/s11837-012-0547-2.
[47] X. He, Y. Shen, Modeling the evolution of interface morphologies in metallic layered composites, JOM 67 (2015) 1486–1490, doi:10.1007/s11837-015-1419-3.
[48] J. Wang, P.M. Anderson, Pinch-off maps for the design of morphologically stable multilayer thin films with immiscible phases, Acta Mater. 53 (2005) 5089–5099.
[49] G. Sharma, R.V. Ramanujan, G.P. Tiwari, Instability mechanisms in lamellar microstructures, Acta Mater. 48 (2000) 875–889.
[50] L.Y. Lin, T.H. Courtney, K.M. Ralls, Deformation induced microstructural instability in the Pb-Sn eutectic, Acta Metall. 25 (1977) 99–106.

[51] L.Y. Lin, T.H. Courtney, Direct observations of lamellar fault migration in the Pb-Sn eutectic, Metall. Trans. 5 (1974) 513–514.
[52] P. Troche, J. Hoffmann, K. Heinemann, F. Hartung, G. Schmitz, H.C. Freyhardt, D. Rudolph, J. Thieme, P. Guttmann, Thermally driven shape instabilities of Nb/Cu multilayer structures: instability of Nb/Cu multilayers, Thin Solid Films 353 (1999) 33–39.
[53] A.S. Budiman, N. Li, Q. Wei, J.K. Baldwin, J. Xiong, H. Luo, D. Trugman, Q.X. Jia, N. Tamura, M. Kunz, K. Chen, A. Misra, Growth and structural characterization of epitaxial Cu/Nb multilayers, Thin Solid Films 519 (2011) 4137–4143.
[54] D. Josell, W.C. Carter, J.E. Bonevich, Stability of multilayer structures: capillary effects, Nanostruct. Mater. 12 (1999) 387–390.
[55] A. Misra, R.G. Hoagland, H. Kung, Thermal stability of self-supported nanolayered Cu/Nb films, Philos. Mag. 84 (2004) 1021–1028.
[56] D. Josell, S.R. Coriell, G.B. McFadden, Evaluating the zero creep conditions for thin film and multilayer thin film specimens, Acta Metall. Mater. 43 (1995) 1987–1999.
[57] J.S. Riano, A.M. Hodge, Exploring the microstructural evolution of Hf-Ti: from nanometallic multilayers to nanostructures, Scr. Mater. 142 (2018) 55–60.
[58] Y.J. Ma, Y.P. Cai, G.J. Wang, M.J. Cui, C. Sun, Z.H. Cao, X.K. Meng, Enhanced thermal stability by heterogeneous interface and columnar grain in nanoscale Cu/Ru multilayers, Mater. Sci. Eng. 742 (2019) 751–759.
[59] M. Hecker, J. Thomas, D. Tietjen, S. Baunack, C.M. Schneider, A. Qiu, N. Cramer, R.E. Camley, Z. Celinski, Thermally induced modification of GMR in Co/Cu multilayers: correlation among structural, transport, and magnetic properties, J. Phys. D Appl. Phys. 36 (2003) 564–572.
[60] H.J. Frost, C.V. Thompson, D.T. Walton, Simulation of thin film grain structures—I. Grain growth stagnation, Acta Metall. Mater. 38 (1990) 1455–1462.
[61] W.W. Mullins, The effect of thermal grooving on grain boundary motion, Acta Metall. 6 (1958) 414–427.
[62] A. Misra, R.G. Hoagland, Effects of elevated temperature annealing on the structure and hardness of copper/niobium nanolayered films, J. Mater. Res. 20 (2005) 2046–2054.
[63] H. Abrams, Grain size measurement by the intercept method, Metallography 4 (1971) 59–78.
[64] J. Hsieh, S. Hung, The effect of Cu:Ag atomic ratio on the properties of sputtered Cu–Ag alloy thin films, Materials 9 (2016).
[65] K.P. Almtoft, A.M. Ejsing, J. Bøttiger, J. Chevallier, N. Schell, R.M.S. Martins, The dependence of the nanostructure of magnetron sputtered Cu–Ag alloy films on composition and temperature, J. Mater. Res. 22 (2007) 1018–1023.
[66] D. Josell, F. Spaepen, Surfaces, interfaces, and changing shapes in multilayered films, MRS Bull. 24 (1999) 39–43.
[67] W.W. Mullins, P.G. Shewmon, The kinetics of grain boundary grooving in copper, Acta Metall. 7 (1959) 163–170.
[68] W.W. Mullins, Theory of thermal grooving, J. Appl. Phys. 28 (1957) 333–339.
[69] M.D. Thouless, Effect of surface diffusion on the creep of thin films and sintered arrays of particles, Acta Metall. Mater. 41 (1993) 1057–1064.
[70] T. Xin, H. Wong, Grain-boundary grooving by surface diffusion with strong surface energy anisotropy, Acta Mater. 51 (2003) 2305–2317.
[71] W. Zhang, J.H. Schneibel, Numerical simulation of grain-boundary grooving by surface diffusion, Comput. Mater. Sci. 3 (1995) 347–358.
[72] W. Zhang, P. Sachenko, I. Gladwell, Thermal grain boundary grooving with anisotropic surface free energies, Acta Mater. 52 (2004) 107–116.
[73] L. Klinger, Surface evolution in two-component system, Acta Mater. 50 (2002) 3385–3395.
[74] H.L. Knoedler, G.E. Lucas, C.G. Levi, Morphological stability of copper-silver multilayer thin films at elevated temperatures, Metall. Mater. Trans. A 34 (2003) 1043–1054.
[75] M.J. Rost, Comment on “Kinetics of voiding and agglomeration of copper nanolayers on silica, Phys. Rev. B 87 (2013) 37401.
[76] H.L. Knoedler, G.E. Lucas, C.G. Levi, Morphological stability of copper-silver multilayer thin films at elevated temperatures: physical metallurgical and materials science, Metall. Mater. Trans. 34A (2003) 1043–1054.
[77] D.W. James, G.M. Leak, Grain boundary diffusion of iron, cobalt and nickel in alpha-iron and of iron in gamma-iron, Philos. Mag. 12 (1965) 491–503.
[78] A. Inoue, H. Nitta, Y. Iijima, Grain boundary self-diffusion in high purity iron, Acta Mater. 55 (2007) 5910–5916.
[79] A. Häßner, Untersuchung der Korngrenzendiffusion von Zn-65 in α-Aluminium-Zink-Legierungen, Krist. Tech. 9 (1974) 1371–1388.
[80] R.E. Hoffman, D. Turnbull, Lattice and grain boundary self-diffusion in silver, J. Appl. Phys. 22 (1951) 634–639.
[81] R. Monzen, K. Kita, Ostwald ripening of spherical Fe particles in Cu-Fe alloys, Philos. Mag. Lett. 82 (2002) 373–382.
[82] S. Lu, Q.-M. Hu, M.P.J. Punkkinen, B. Johansson, L. Vitos, First-principles study of fcc-Ag/bcc-Fe interfaces, Phys. Rev. B 87 (2013) 224104.
[83] D.A. Porter, K.E. Easterling, Phase Transformations in Metals and Alloys, Chapman & Hall, 1992.
[84] F.Y. Genin, W.W. Mullins, P. Wynblatt, Capillary instabilities in thin films: A model of thermal pitting at grain boundary vertices, Acta Metall. Mater. 40 (1992) 3239–3248.
[85] N. Gazit, L. Klinger, E. Rabkin, Chemically-induced solid-state dewetting of thin Au films, Acta Mater. 129 (2017) 300–311.
[86] D. Amram, L. Klinger, N. Gazit, H. Gluska, E. Rabkin, Grain boundary grooving in thin films revisited: The role of interface diffusion, Acta Mater. 69 (2014) 386–396.
[87] F.Y. Genin, W.W. Mullins, P. Wynblatt, The effect of stress on grain boundary grooving, Acta Metall. Mater. 41 (1993) 3541–3547.
[88] H.J. Vogel, L. Ratke, Instability of grain boundary grooves due to equilibrium grain boundary diffusion, Acta Metall. Mater. 39 (1991) 641–649.
[89] D.A. Porter, K.E. Easterling, Phase transformations in metals and alloys (revised reprint), CRC press, 2009.
[90] A.P. Sutton, R. W. Baulluffi, Interfaces in crystalline materials, monographs on the physice and chemistry of materials. (1995) 414–423.